

MoDAI: Self-Supervised Neural Modality Discovery via Decorrelation for Speech Neuroprosthesis

Yuanhao Chen
yc.th@dartmouth.edu
Dartmouth College
Hanover, NH, USA

Peter Chin
pc@dartmouth.edu
Dartmouth College
Hanover, NH, USA

Abstract

Speech neuroprosthesis systems decode intended speech from neural activity in the absence of audible output, offering a path to restoring communication for individuals with speech-impairing conditions. Current approaches decode predominantly from motor cortical areas, discarding others—such as area 44, part of Broca’s area—that may encode complementary linguistic information. We introduce **MoDAI** (**M**odality **D**ecorrelation and **A**lignment), a framework that discovers complementary neural modalities through the interplay of two objectives in a shared projection space. A contrastive loss aligns each of several parallel brain encoders with the text embeddings of a pretrained large language model (LLM), while a decorrelation loss prevents the encoders from coalescing to duplicative representations. We prove that these objectives are in productive tension: Contrastive alignment induces transitive modality coalescence, which decorrelation must counteract for the framework to discover diverse neurolinguistic modalities. On the Brain-to-Text Benchmark ’24, MoDAI reduces word error rate (WER) from 26.3% to 21.6% compared to the previous best end-to-end method, with the gain from incorporating previously discarded area 44 signals arising entirely from the decorrelation mechanism. Analysis of the discovered modalities reveals functional specialization: Encoders receiving area 44 input capture structural and syntactic properties (sentence length, grammatical voice, wh-words), consistent with the neurolinguistic understanding of Broca’s area.

CCS Concepts

• **Computing methodologies** → **Learning paradigms; Machine learning approaches**; • **Human-centered computing** → *Human computer interaction (HCI); Accessibility technologies*.

Keywords

Speech neuroprosthesis, self-supervised learning, multimodal learning, neurolinguistics, brain-computer interfaces

1 Introduction

Speech is an essential modality of human communication, and restoring it for individuals who have lost the ability to speak is a central goal of assistive technology. Speech neuroprosthesis—the decoding of intended speech from neural activity in the absence of audible output—has emerged as a promising direction for brain-computer interfaces (BCIs) that could restore communication to people with conditions such as amyotrophic lateral sclerosis (ALS) or locked-in syndrome [19, 22, 24]. As an interface that transduces neural signals into language, speech neuroprosthesis is inherently a multimodal interaction problem and directly addresses the inclusivity goals of the human-computer interaction (HCI) community:

enabling natural, high-bandwidth communication for users who cannot access conventional speech or gesture-based interfaces.

Current speech neuroprosthesis systems decode speech almost exclusively from motor signals, leveraging the well-characterized mapping between neural activity and the movements of the tongue, lips, jaw, and larynx [4, 19, 24]. However, speech production involves more than articulators. Broca’s area (including area 44) has long been associated with higher-level language functions including syntactic processing, phonological planning, and semantic retrieval [10, 23], yet its signals are discarded by all prior work on the Brain-to-Text Benchmark ’24 because they do not improve phoneme decoding [8, 17, 24, 26]. This raises a question: *Can area 44 signals contribute to speech neuroprosthesis if the system is designed to discover and exploit **complementary neurolinguistic modalities** rather than treating all neural signals as a single articulatory stream?*

In standard multimodal contrastive learning [12, 21], the modalities—text, image, audio, video—are predefined, and each has its own dedicated encoder. Decorrelation between modalities is not a concern because the inputs are already categorically distinct. In the neural setting, by contrast, the cortical signals from area 6v and area 44 are recorded from physically adjacent, intercorrelated electrode arrays, and there is no a priori labeling of which neural patterns constitute distinct “modalities.” Willett et al. [24] show that area 44 electrodes do encode sparse articulatory information, so simply feeding all channels into a single encoder can lead to redundancy with area 6v signals rather than complementary specialization.

We introduce **MoDAI** (**M**odality **D**ecorrelation and **A**lignment), a framework that addresses this challenge through the interplay of two objectives in a shared projection space. A contrastive loss aligns each parallel brain encoder with the text embeddings of a pretrained large language model (LLM), anchoring all modalities to a common linguistic reference. We prove that this alignment creates a transitive pressure for all modality projections to coalesce (Proposition 3.1), which would collapse the encoders into redundant copies. A decorrelation loss counteracts this coalescence by penalizing feature-wise correlation between encoder pairs (Proposition 3.2). By operating in a shared projection space, the two losses are kept in productive tension: Contrastive alignment prevents the decorrelation projector from collapsing trivially, while decorrelation prevents the encoders from coalescing.

Applying MoDAI to the Brain-to-Text Benchmark ’24 dataset, we show that three parallel brain encoders—trained end-to-end with an LLM decoder—discover complementary modalities that reduce word error rate (WER) from 26.3% to 21.6%, improving over the previous best end-to-end (E2E) method by 4.7 percentage points

on the test set and approaching the performance of cascaded systems that require separately trained language models. Crucially, the improvement from adding the previously discarded area 44 signals (MoDAL-1 \rightarrow MoDAL-Full) is 0.8 percentage points—a statistically significant gain that arises entirely from the decorrelation mechanism, since without it, area 44 adds no benefit. Linear probes reveal that the novel encoders specialize in structural and syntactic properties (sentence length, voice, wh-words) rather than articulatory features, consistent with the neurolinguistic understanding of Broca’s area. Our contributions are as follows:

- (1) We propose MoDAL, a framework for self-supervised neural modality discovery that uses contrastive alignment and decorrelation in a shared projection space. We prove that these objectives are in productive tension: Contrastive alignment induces transitive modality coalescence, which decorrelation must counteract to encourage complementary specialization.
- (2) We demonstrate that area 44 (part of Broca’s area) signals, discarded by all prior work on this dataset, carry complementary linguistic information that MoDAL can discover and exploit, reducing WER by 4.7 percentage points relative to the previous best E2E method.
- (3) We provide a detailed analysis of the discovered modalities through cross-correlation measurement, retrieval, canonical correlation analysis, and linear probing for linguistic properties, showing that the parallel encoders specialize in different linguistic features consistent with the known functional roles of their respective brain areas.

2 Related Work

2.1 Speech Neuroprosthesis

Intracortical BCIs for speech decoding have advanced rapidly in recent years. Willett et al. [24] demonstrated the first high-performance speech neuroprosthesis for a participant with ALS, using an recurrent neural network (RNN) decoder on area 6v neural activity followed by an n -gram language model, achieving 23.8% WER on a 125,000-word vocabulary in real time. Metzger et al. [19] developed a similar cascaded system for a participant with anarthria. Card et al. [4] introduced rapid calibration methods that reduce the data requirements for new users. These cascaded systems separate phoneme decoding from language modeling, requiring independently trained components and beam search re-scoring at inference time.

End-to-end approaches that directly map neural signals to text through a single differentiable model have emerged as an alternative. Feng et al. [8] proposed the first E2E framework for this dataset, using a gated recurrent unit (GRU) encoder with a LLM decoder fine-tuned via quantized low-rank adaptation (QLoRA). Zhang et al. [26] introduced BIT, using a transformer encoder pre-trained on cross-species motor signals to achieve strong results in both cascaded and E2E settings. Fiedler et al. [9] adapted the self-supervised wav2vec 2.0 speech framework [3] to neural signals, treating brain activity as a “language” to be learned.

All of these methods decode exclusively from ventral premotor cortex (area 6v), which encodes articulator movements. None exploit signals from area 44 (part of Broca’s area), which Willett

et al. [24] found to degrade phoneme decoding. However, neuroscience evidence suggests that Broca’s area plays a role in higher-level language processing—including syntactic structure, semantic retrieval, and phonological planning—distinct from articulatory representations in the motor cortex [10, 23]. Verwoert et al. [23] recently showed through whole-brain intracranial recordings that the inferior frontal cortex (containing Broca’s area) was correlated almost exclusively with semantic rather than articulatory or acoustic speech representations. They noted that its indirect connection to low-level speech features “*limit[s] its use for an articulatory-based speech neuroprosthesis.*” Our work tests whether a framework designed for modality *discovery*—rather than articulatory decoding—can recover this complementary information.

2.2 Multimodal Learning

Contrastive learning has become the dominant approach for aligning representations across modalities. CLIP [21] demonstrated that image and text encoders trained with a symmetric InfoNCE loss produce a joint embedding space with strong zero-shot transfer capabilities. ImageBind [12] explores using image as an anchor modality, showing that aligning each new modality (audio, depth, thermal, inertial measurement unit) to image via pairwise contrastive losses induces *emergent* alignment between modalities that were never paired during training—a transitive property of shared embedding spaces.

A key assumption in these methods is that the modalities are *predefined*: Each has a distinct physical origin (camera, microphone, depth sensor), dedicated encoder, and typically abundant paired data. Decorrelation between modalities is not needed because the inputs are already categorically distinct—an image and its caption share semantic content but are never at risk of encoding identical low-level features. In our setting, the parallel brain encoders receive signals from physically adjacent, intercorrelated cortical arrays [24], making inter-modality redundancy the default outcome rather than an exceptional failure mode.

Self-supervised decorrelation methods provide the complementary tool we need. Barlow Twins [25] introduced a cross-correlation-based loss that drives augmented views of the same input toward invariant but non-redundant representations by pushing the cross-correlation matrix toward the identity. Our decorrelation loss adapts this idea to the inter-modality setting: Instead of targeting identity (invariance), we target zero diagonal (decorrelation), and we compute the cross-correlation *between* different modality encoders rather than between augmented views. Moreover, we show that this loss must operate in a shared projection space with the contrastive loss to be effective; a separate decorrelation projector collapses trivially (Table 4).

MoDAL combines these two traditions—contrastive alignment from multimodal learning and decorrelation from self-supervised learning—to address a problem that neither solves alone: discovering complementary modalities from intercorrelated neural signals without predefined modality labels.

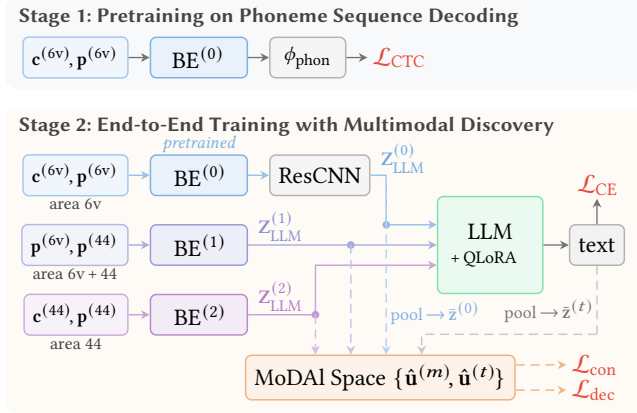


Figure 1: MoDAL architecture. Stage 1 pretrains brain encoder $BE^{(0)}$ on phonemes with CTC loss. In Stage 2, three parallel brain encoders feed a QLoRA-adapted LLM decoder (solid), while branching into the shared MoDAL projection space with text (dashed) for contrastive alignment and decorrelation.

3 Method

3.1 Dataset

We use the Brain-to-Text Benchmark '24 dataset [24], which contains attempted speech recordings from participant T12, a woman with bulbar-onset ALS and unable to produce intelligible speech. The dataset comprises 12,100 large-vocabulary sentences collected across 25 recording sessions spanning approximately four months.

Preprocessing. Neural activity was recorded from four 64-electrode Utah microelectrode arrays (256 electrodes total): two implanted in ventral premotor cortex (area 6v) and two in the ventral portion of area 44, part of Broca’s area. For each cortical area, two signal types are provided in 20 ms time bins: threshold crossing counts $c^{(44)}, c^{(6v)}$ and spike band power $p^{(44)}, p^{(6v)}$. Blockwise z-scoring is applied to mitigate recording nonstationarities. Following Willett et al. [24], we stack each sequence with a kernel of $k=14$ bins and stride $s=4$ to yield patches of 280 ms with 200 ms overlap, giving $D_{\text{in}} = 64k = 896$ features per signal type.

Previously Discarded Area 44 Signals. Previous studies on this dataset decode speech exclusively from area 6v. Willett et al. [24] report that area 44 contains little production-related information and that including it degrades decoding performance; subsequent works have likewise discarded area 44 entirely [8, 9, 17, 26]. A central question of this work is whether area 44 signals carry complementary linguistic information that can be recovered through self-supervised modality discovery and leveraged by an LLM decoder.

3.2 Architecture

3.2.1 Articulatory Brain Encoder. The only component trained in Stage 1 is a brain encoder that maps area 6v neural activity to articulatory features for phoneme decoding. GRU-based encoders were adopted following prior work on this benchmark, which found that GRUs outperform LSTM and transformer alternatives [9, 17].

We additionally apply channel-wise locked dropout [11] to the input features and layer normalization [2] to the recurrent outputs, which we find improves generalization to held-out sessions.

To accommodate neural nonstationarities across recording sessions, we apply a day-specific affine input projection indexed by session day d followed by Softsign activation:

$$\mathbf{X}' = \phi_{\text{in}}^{(d)}(\mathbf{X}) = \text{Softsign}(\mathbf{X}\mathbf{W}_{\text{in}}^{(d)\top} + \mathbf{b}_{\text{in}}^{(d)}) \in \mathbb{R}^{B \times T \times 2D_{\text{in}}},$$

where \mathbf{X} concatenates $c^{(6v)}$ and $p^{(6v)}$, hence $2D_{\text{in}}$.

Channel-wise locked dropout randomly zeros entire channels uniformly across time steps, encouraging the model to distribute its representation broadly rather than overfitting to a subset of electrodes. The core encoder is a stack of 5 bidirectional GRU layers with layer normalization on the output:

$$\mathbf{Y} = (\text{LN} \circ \text{BiGRU} \circ \text{Drop}_{\text{chan}})(\mathbf{X}') \in \mathbb{R}^{B \times T \times 2D_{\text{GRU}}},$$

where $2D_{\text{GRU}}$ reflects the concatenation of forward and backward hidden states. The per-frame outputs are projected onto $|\mathcal{P}| = 44$ phoneme tokens for connectionist temporal classification (CTC) decoding: $\mathbf{Z}_{\text{phon}} = \phi_{\text{phon}}(\mathbf{Y}) \in \mathbb{R}^{B \times T \times |\mathcal{P}|}$.

3.2.2 Parallel Brain Encoders for Multimodal Discovery. In Stage 2, we add parallel brain encoders, each with a separate affine head mapping its outputs into the LLM embedding space: $\mathbf{Z}_{\text{LLM}}^{(m)} = \phi_{\text{LLM}}^{(m)}(\mathbf{Y}^{(m)}) \in \mathbb{R}^{B \times T \times D_{\text{LLM}}}$, where superscript (m) indexes the brain encoder modality. In our full model, we have three brain encoders: one for area 6v, one for both areas, and one for area 44.

$$\mathbf{Z}_{\text{LLM}}^{(m)} = \text{BE}^{(m)}(\mathbf{X}^{(m)}), \quad m \in \{0, 1, 2\},$$

$$\text{where } \text{BE}^{(m)} = \phi_{\text{LLM}}^{(m)} \circ \text{LN} \circ \text{BiGRU} \circ \text{Drop}_{\text{chan}} \circ \phi_{\text{in}}^{(m,d)},$$

$$\text{and } \mathbf{X}^{(0)} = \begin{bmatrix} \mathbf{c}_{1:T}^{(6v)} \\ \mathbf{p}_{1:T}^{(6v)} \end{bmatrix}, \quad \mathbf{X}^{(1)} = \begin{bmatrix} \mathbf{p}_{1:T}^{(6v)} \\ \mathbf{p}_{1:T}^{(44)} \end{bmatrix}, \quad \mathbf{X}^{(2)} = \begin{bmatrix} \mathbf{c}_{1:T}^{(44)} \\ \mathbf{p}_{1:T}^{(44)} \end{bmatrix}.$$

$BE^{(0)}$ is initialized from the pretrained Stage 1 encoder; the others share its architecture but are randomly initialized. Due to limited computational resources, only three parallel encoders are used, and $BE^{(1)}$ receives only spike power features, which are more robust and informative than threshold crossings for area 6v [24].

Temporal Residual CNN. The articulatory encoder $BE^{(0)}$ captures phoneme-level motor dynamics, so its full per-frame output $\mathbf{Z}_{\text{LLM}}^{(0)} \in \mathbb{R}^{B \times T \times D_{\text{LLM}}}$ is retained as a token sequence for the LLM decoder. To refine these representations, we apply a temporal residual convolutional neural network (CNN):

$$\mathbf{Z}_{\text{LLM}}^{(0)} \stackrel{\text{redef}}{=} (\phi_{\text{ref}} \circ \text{GELU} \circ \text{ResCNN})(\mathbf{Z}_{\text{LLM}}^{(0)}),$$

where $\text{ResCNN}(\mathbf{Z}) = \mathbf{Z} + (\text{LN} \circ \text{Conv}_2 \circ \text{GELU} \circ \text{Conv}_1)(\mathbf{Z})$ uses kernel size 5 and dilation 2, giving an effective receptive field of 17 frames (≈ 272 ms) that captures coarticulatory transitions between adjacent phonemes.

Unlabeled Utterance-Level Modalities. Unlike the articulatory encoder, $BE^{(1)}$ and $BE^{(2)}$ are designed to discover complementary modalities through self-supervised decorrelation, without phoneme supervision. The information these encoders may capture—e.g., sentence-level semantics or syntactic structure—is not expected to

be frame-aligned. Accordingly, we represent each new modality as a single vector:

$$\mathbf{Z}_{\text{LLM}}^{(m)} \stackrel{\text{redef}}{=} \phi_{\text{LLM}}^{(m)}(\mathbf{Y}_T^{(m)}) \in \mathbb{R}^{B \times 1 \times D_{\text{LLM}}}, \quad m \in \{1, 2\},$$

where $\mathbf{Y}_T^{(m)}$ is the final hidden state of the BiGRU stack. These vectors are appended to the articulatory token sequence as global conditioning signals for the LLM decoder. Empirically, passing full sequence outputs from the new encoders destabilizes training—likely because multiple unsupervised token streams create redundant temporal signals with no phoneme-level anchor—whereas utterance-level summaries avoid this while preserving the capacity to encode abstract linguistic information.

3.2.3 Multimodal LLM Decoder. The decoder is a pretrained LLM (Aero-1-Audio-1.5B [16]) that autoregressively generates the transcription conditioned on the brain encoder outputs. The input embedding sequence concatenates the encoder representations with a tokenized text prompt and, during training, the target transcription:

$$\mathbf{E} = \left[\mathbf{Z}_{\text{LLM}}^{(0)} \mid \mathbf{Z}_{\text{LLM}}^{(1)} \mid \mathbf{Z}_{\text{LLM}}^{(2)} \mid \mathbf{E}_{\text{prompt}} \mid \mathbf{E}_{\text{target}} \right]$$

where $\mathbf{Z}_{\text{LLM}}^{(0)} \in \mathbb{R}^{B \times T \times D_{\text{LLM}}}$ is the articulatory token sequence, $\mathbf{Z}_{\text{LLM}}^{(1)}, \mathbf{Z}_{\text{LLM}}^{(2)} \in \mathbb{R}^{B \times 1 \times D_{\text{LLM}}}$ are the utterance-level features, and $\mathbf{E}_{\text{prompt}}, \mathbf{E}_{\text{target}}$ are the token embeddings of the text prompt and target sentence. Each encoder output occupies a separate conversational turn using the LLM’s chat template, so the model can attend to each modality as a distinct input segment. The text prompt instructs the model to transcribe the preceding neural signals. During inference, $\mathbf{E}_{\text{target}}$ starts empty and the model generates tokens autoregressively.

To adapt the LLM while preserving its pretrained language capabilities, we freeze all base parameters and apply QLoRA [7, 15] with 4-bit NormalFloat quantization. Low-rank adapters ($r=16$, $\alpha=32$) are inserted into all linear projections ([kv]_proj, [gate|up|down]_proj). The brain encoders, projection heads, and LoRA adapters are the only trainable components in Stage 2.

3.3 Training Objectives

3.3.1 Stage 1: Phoneme Decoding with CTC Loss. In Stage 1 we train the articulatory encoder $\text{BE}^{(0)}$ with the CTC loss [13] to predict phoneme sequences from area 6v neural activity. Let $\mathbf{p} = (p_1, \dots, p_L)$ denote the target phoneme sequence and let $\mathcal{B}^{-1}(\mathbf{p})$ be the set of frame-level alignments that reduce to \mathbf{p} under the CTC collapsing function \mathcal{B} . The loss marginalizes over all valid alignments:

$$\mathcal{L}_{\text{CTC}} = -\log \sum_{\pi \in \mathcal{B}^{-1}(\mathbf{p})} P(\pi \mid \mathbf{Z}_{\text{phon}}).$$

Only $\text{BE}^{(0)}$ and ϕ_{phon} are trained in this stage; the LLM is not involved.

3.3.2 Stage 2: End-to-End Training with Multimodal Discovery. In Stage 2, the full pipeline is trained end-to-end with a composite objective:

$$\mathcal{L} = \mathcal{L}_{\text{CE}} + \lambda_{\text{con}}(s) \mathcal{L}_{\text{con}} + \lambda_{\text{dec}}(s) \mathcal{L}_{\text{dec}},$$

where \mathcal{L}_{CE} is the cross-entropy loss for transcription, \mathcal{L}_{con} is a contrastive alignment loss, \mathcal{L}_{dec} is a decorrelation loss, and $\lambda_{\text{con}}(s), \lambda_{\text{dec}}(s)$ are step-varying weights defined below.

Cross-Entropy Loss. The LLM decoder is trained with standard next-token cross-entropy on the target transcription $\mathbf{y} = (y_1, \dots, y_L)$:

$$\mathcal{L}_{\text{CE}} = -\frac{1}{L} \sum_{l=1}^L \log P(y_l \mid \mathbf{E}_{<l}),$$

where $\mathbf{E}_{<l}$ denotes all preceding input embeddings (neural tokens, prompt tokens, and previously generated target tokens). This is the primary training signal that teaches the LLM to transduce neural representations into text.

Shared MoDAL Projection Space. The contrastive and decorrelation losses operate in a shared projection space $\mathbb{R}^{D_{\text{MoDAL}}}$ (the *MoDAL space*), separate from the LLM embedding space to avoid disrupting its geometry. For each brain encoder modality m and for text t , we first obtain a single vector per sample by mean-pooling across time (a no-op for utterance-level $\text{BE}^{(1,2)}$):

$$\bar{\mathbf{z}}_i^{(\cdot)} = \text{pool}(\mathbf{Z}_{\text{LLM},i}^{(\cdot)}) \in \mathbb{R}^{D_{\text{LLM}}},$$

then map each into the MoDAL space via modality-specific affine projections:

$$\mathbf{u}_i^{(\cdot)} = \phi_{\text{MoDAL}}^{(\cdot)}(\bar{\mathbf{z}}_i^{(\cdot)}) \in \mathbb{R}^{D_{\text{MoDAL}}}, \quad (\cdot) \in \{0, 1, 2, t\}.$$

A critical design choice is that both losses share the same projection weights $\phi_{\text{MoDAL}}^{(\cdot)}$ and per-sample L2 normalization, yielding

$$\hat{\mathbf{u}}_i^{(\cdot)} = \mathbf{u}_i^{(\cdot)} / \|\mathbf{u}_i^{(\cdot)}\| \in \mathbb{S}^{D_{\text{MoDAL}}-1}.$$

The contrastive loss operates on these unit vectors directly. The decorrelation loss applies an additional per-feature batch standardization (centering and scaling each dimension to zero mean and unit variance across the batch) to obtain $\check{\mathbf{u}}_i^{(m)}$, so that the cross-correlation matrix $\mathbf{C}^{(m,n)}$ yields Pearson correlations. If separate projectors were used for each loss, the decorrelation projector could map all samples to a constant vector—producing the zero matrix after batch standardization and trivially minimizing \mathcal{L}_{dec} without decorrelating the encoders. Sharing projections prevents this: The contrastive loss requires sample-discriminative projections, precluding constant-map collapse and ensuring that decorrelation is computed over text-relevant directions (validated by ablations in Tables 2 and 4). The shared L2 normalization further ensures both losses measure angular relationships in the same geometry, preventing an encoder from satisfying decorrelation through magnitude differences alone.

Contrastive Loss. The contrastive loss aligns each brain encoder with the text representation via a symmetric InfoNCE objective [20]. For modality m and sample i :

$$\ell_i^{(m \rightarrow t)} = -\log \frac{e^{\hat{\mathbf{u}}_i^{(m)} \cdot \hat{\mathbf{u}}_i^{(t)} / \tau}}{\sum_j e^{\hat{\mathbf{u}}_i^{(m)} \cdot \hat{\mathbf{u}}_j^{(t)} / \tau}}, \quad \ell_i^{(t \rightarrow m)} = -\log \frac{e^{\hat{\mathbf{u}}_i^{(t)} \cdot \hat{\mathbf{u}}_i^{(m)} / \tau}}{\sum_j e^{\hat{\mathbf{u}}_i^{(t)} \cdot \hat{\mathbf{u}}_j^{(m)} / \tau}},$$

where τ is a learnable temperature parameter. The total contrastive loss symmetrizes over directions and averages over modalities:

$$\mathcal{L}_{\text{con}} = \frac{1}{M} \sum_{m=1}^M \frac{1}{2B} \sum_{i=1}^B [\ell_i^{(m \rightarrow t)} + \ell_i^{(t \rightarrow m)}].$$

Each modality is independently aligned with text; no direct inter-modality pairing is enforced.

Contrastive Transitivity. Although the contrastive loss pairs each modality independently with text, all modalities share the same text projector $\phi_{\text{MoDAL}}^{(t)}$ and therefore the same text targets $\hat{\mathbf{u}}_i^{(t)}$. This creates a transitive alignment pressure: driving each $\hat{\mathbf{u}}_i^{(m)}$ toward $\hat{\mathbf{u}}_i^{(t)}$ simultaneously drives all modalities toward each other.

PROPOSITION 3.1 (CONTRASTIVE TRANSITIVITY). *Let $\{\hat{\mathbf{u}}_i^{(t)}\}_{i=1}^B \subset \mathbb{S}^{D_{\text{MoDAL}}-1}$ be fixed, pairwise distinct text projections. In the low-temperature regime ($\tau \rightarrow 0^+$), the unique minimizer of \mathcal{L}_{con} over all $\hat{\mathbf{u}}_i^{(m)} \in \mathbb{S}^{D_{\text{MoDAL}}-1}$ satisfies $\hat{\mathbf{u}}_i^{(m)} = \hat{\mathbf{u}}_i^{(t)}$ for all $m \in [M]$ and $i \in [B]$. Consequently, $\hat{\mathbf{u}}_i^{(m)} = \hat{\mathbf{u}}_i^{(n)}$ for all modality pairs (m, n) and all samples i .*

The proof is given in Appendix A. For practical (small but finite) temperatures, the same directional pressure applies: The contrastive gradient drives each $\hat{\mathbf{u}}_i^{(m)}$ toward $\hat{\mathbf{u}}_i^{(t)}$, so the qualitative conclusion holds throughout training.

Decorrelation Loss. To encourage the brain encoders to learn diverse representations, the decorrelation loss counteracts the coalescence described above by penalizing statistical dependence between modality pairs. Starting from $\hat{\mathbf{u}}_i^{(m)}$, we apply per-feature batch standardization to obtain $\check{\mathbf{u}}_i^{(m)}$ and compute the empirical cross-correlation matrix:

$$\mathbf{C}^{(m,n)} = \frac{1}{B} \check{\mathbf{U}}^{(m)\top} \check{\mathbf{U}}^{(n)} \in \mathbb{R}^{D_{\text{MoDAL}} \times D_{\text{MoDAL}}},$$

where $\check{\mathbf{U}}^{(m)} \in \mathbb{R}^{B \times D_{\text{MoDAL}}}$ stacks the standardized projections and the diagonal entry $C_{ii}^{(m,n)}$ gives the Pearson correlation between feature i across the two modalities. The decorrelation loss penalizes only these diagonal entries:

$$\mathcal{L}_{\text{dec}} = \frac{2}{M(M-1)} \sum_{0 \leq m < n < M} \frac{1}{D_{\text{MoDAL}}} \sum_{i=1}^{D_{\text{MoDAL}}} (C_{ii}^{(m,n)})^2.$$

This is inspired by Barlow Twins [25], but adapted for inter-modality comparison: The cross-correlation is computed *between* different modality encoders rather than between augmented views, and the diagonal target is zero (decorrelation) rather than one (invariance). We omit the off-diagonal penalty $\sum_{i \neq j} (C_{ij}^{(m,n)})^2$: At the contrastive equilibrium where $\check{\mathbf{U}}^{(m)} = \check{\mathbf{U}}^{(n)}$, the off-diagonal entries reduce to *within*-modality feature correlations, which regularize for feature independence but do not enforce the inter-modality decorrelation we seek. The diagonal alone directly measures whether corresponding text-aligned features carry redundant information across modalities.

PROPOSITION 3.2 (DECORRELATION AT THE CONTRASTIVE FIXED POINT). *If $\hat{\mathbf{u}}_i^{(m)} = \hat{\mathbf{u}}_i^{(n)}$ for all $i \in [B]$ (the contrastive equilibrium from Proposition 3.1), then after batch-wise feature standardization, $C_{ii}^{(m,n)} = 1$ for all $i \in [D_{\text{MoDAL}}]$, and the decorrelation loss achieves its maximum value of 1.*

Propositions 3.1 and 3.2 (proofs in Appendix A) together establish that the contrastive and decorrelation losses are in *productive tension*: The contrastive loss drives $C_{ii}^{(m,n)} \rightarrow 1$ (via transitive alignment through text), while the decorrelation loss drives $C_{ii}^{(m,n)} \rightarrow 0$. At equilibrium, each encoder must maintain sufficient alignment

with text to support the transcription task (\mathcal{L}_{CE}) while encoding *different* text-relevant information from the other encoders. This is the mechanism by which modality discovery emerges without explicit modality labels.

Loss Warmup. The contrastive and decorrelation loss weights are linearly warmed up from zero: $\lambda_{\text{con}}(s) = (s/s_{\text{max}}) \lambda_{\text{con}}$ and $\lambda_{\text{dec}}(s) = (s/s_{\text{max}}) \lambda_{\text{dec}}$, where s is the current optimizer step and s_{max} the total number of steps. This ensures that \mathcal{L}_{CE} establishes a baseline representation before the auxiliary losses begin to shape encoder specialization.

4 Experiments

4.1 Experimental Setup

Data Splits and Evaluation. We use the default partitioning of the Brain-to-Text Benchmark '24 dataset [24]: For each recording day, the first two blocks are reserved as competition holdout, the last block as the test set, and the remaining blocks as training data, yielding 8,780 training, 880 test, and 1,200 holdout sentences. All models are selected based on test-set WER, and only the main experiment is evaluated on the competition holdout due to submission limits. WER measures the minimum edit distance between predicted and reference word sequences, normalized by the reference length:

$$\text{WER} = \frac{S + D + I}{N},$$

where S , D , and I denote the number of substitutions, deletions, and insertions, and N is the number of reference words. We lowercase all text and remove all punctuation except apostrophes before computing WER.

Training. In Stage 1, the articulatory encoder $\text{BE}^{(0)}$ is pretrained with the CTC loss for 300 epochs (peak learning rate 1×10^{-4}). In Stage 2, the full pipeline is trained end-to-end for 150 epochs with the composite objective from Section 3.3.2. We use two learning rate groups: 1.5×10^{-4} for the pretrained $\text{BE}^{(0)}$ and LoRA adapters, and 2×10^{-4} for the randomly initialized modules ($\text{BE}^{(1,2)}$ and projection heads), allowing the new encoders to adapt faster while using the pretrained modalities as stable anchors. Both stages use AdamW [18] with cosine annealing to zero. The complete set of hyperparameters is given in Table 6 (Appendix B). All experiments are run on 8 \times NVIDIA RTX PRO 6000 GPUs with distributed data-parallel training and mixed precision (bfloat16).

4.2 Neural Speech Decoding Results

Table 1 compares MoDAL against prior work. We report *MoDAL-1*, which uses only $\text{BE}^{(0)}$ on area 6v with contrastive alignment to text, and *MoDAL-Full*, which adds $\text{BE}^{(1)}$ and $\text{BE}^{(2)}$ with decorrelation and contrastive alignment.

The improvement over prior E2E work decomposes into two sources. First, MoDAL-1 reduces WER by 3.9 percentage points on the test set and 5.9 on the holdout relative to Feng et al. [8], despite sharing the same two-stage paradigm (CTC pretraining followed by E2E LLM fine-tuning) and BiGRU encoder architecture. This gain is attributable to contrastive alignment with text in the MoDAL space, which provides an auxiliary training signal that improves the encoder representations beyond what cross-entropy alone achieves.

Table 1: WER (%) comparison on the Brain-to-Text Benchmark '24. MoDAL results are mean \pm 95% CI over 5 seeds. All methods use the same dataset and evaluation splits.

Method	Type	Test \downarrow	Holdout \downarrow
Willett et al. [24]	Cascaded	23.8–24.7 [†]	15.4
Feng et al. [8]	E2E	26.3	24.7
MoDAL-1 (ours)	E2E	22.4 \pm 0.2	18.8 \pm 0.5
MoDAL-Full (ours)	E2E	21.6 \pm 0.1	17.7 \pm 0.4

[†] Willett et al. report online WER on their own evaluation sentences (not the benchmark test split), separately for vocal (23.8%; 95% CI 21.8–25.9) and silent (24.7%; 95% CI 22.0–27.4) conditions. We include these as a reference point, noting that the evaluation sentences differ from the benchmark’s test partition.

Table 2: Loss ablation on the test set. WER (%) is mean \pm 95% CI over 5 seeds. All configurations use three brain encoders.

	\mathcal{L}_{CE}	\mathcal{L}_{con}	\mathcal{L}_{dec}	Shared proj.	Test WER \downarrow
1.	✓			n/a	23.9 \pm 0.7
2.	✓	✓		n/a	22.0 \pm 0.1
3.	✓		✓	n/a	26.1 \pm 0.6
4.	✓	✓	✓	×	22.2 \pm 0.3
5.	✓	✓	✓	✓	21.6 \pm 0.1

Second, MoDAL-Full further reduces WER by 0.8 points on the test set and 1.1 on the holdout by incorporating the previously discarded area 44 signals (95% confidence intervals do not overlap; Table 1). This demonstrates that the MoDAL framework can extract complementary information from neural signals that prior methods found uninformative.

On the competition holdout, MoDAL (17.7%) approaches the offline cascaded system of Willett et al. [24] (15.4%), despite fundamental architectural differences: Their system requires a separately trained n -gram language model with beam search re-scoring, whereas MoDAL is a single E2E model that relies on the LLM’s pretrained weights for language modeling. Their online system achieves 23.8–24.7%; while not directly comparable due to different test partitions, MoDAL (21.6%) outperforms this reference point. Language model re-scoring is orthogonal to our modality discovery contribution and could in principle be applied on top of MoDAL to further improve performance.

4.3 Ablation Studies

4.3.1 Loss Ablations. Table 2 isolates the contribution of each loss component. Adding contrastive alignment to the cross-entropy baseline yields the largest single improvement (23.9% \rightarrow 22.0%), confirming that aligning brain encoder representations with text in the MoDAL space substantially improves the learned representations beyond what \mathcal{L}_{CE} alone achieves.

Decorrelation without contrastive alignment (row 3) degrades performance to 26.1%, worse than the CE-only baseline. This validates the theoretical prediction: \mathcal{L}_{dec} is designed to counteract the transitive coalescence induced by \mathcal{L}_{con} (Propositions 3.1–3.2), and

Table 3: Component ablations on the test set. WER (%) is mean \pm 95% CI over 5 seeds. All configurations use the full loss ($\mathcal{L}_{CE} + \mathcal{L}_{con} + \mathcal{L}_{dec}$) in the shared MoDAL space.

Configuration	Test WER \downarrow
1. Sequence output from $BE^{(1,2)}$	24.0 \pm 0.3
2. $BE = \{BE^{(0)}, BE^{(1)}\}$	22.2 \pm 0.3
3. $BE = \{BE^{(0)}, BE^{(2)}\}$	22.3 \pm 0.3
4. $BE = \{BE^{(0)}, BE^{(0)'}\}$ (area 6v only)	22.5 \pm 0.3
5. MoDAL-Full	21.6 \pm 0.1

without that coalescence to push against, the decorrelation loss disrupts the shared structure that the LLM decoder relies on.

When both losses are active but the decorrelation projector is separate from the contrastive projector (row 4), performance is statistically indistinguishable from no decorrelation (row 2), as 95% confidence intervals overlap. Table 4 confirms that the separate projector achieves near-identical cross-correlations to the no-decorrelation baseline—the trivial-collapse failure mode predicted in Section 3.3.2.

Only when all three losses operate in the shared MoDAL space (row 5) does the full benefit emerge: 21.6%, a further 0.4 percentage point improvement. This confirms that productive tension between \mathcal{L}_{con} and \mathcal{L}_{dec} in a shared space is the mechanism that enables discovery of complementary modalities from the previously discarded area 44 signals.

We also find that the auxiliary losses are sensitive to batch size: Halving it to $B=64$ erases their benefit entirely, matching the CE-only baseline (Appendix C).

4.3.2 Component Ablations. Table 3 ablates the parallel encoder design. Replacing the utterance-level representation of $BE^{(1,2)}$ with full sequence output (row 1) causes the largest degradation (24.0%), confirming that multiple unsupervised token streams destabilize training as discussed in Section 3.2.2: The novel encoders are expected to capture utterance-level linguistic structure rather than frame-aligned articulatory dynamics, and a single conditioning vector per encoder is sufficient to convey this information to the LLM decoder.

Dropping either novel encoder (rows 2–3) yields similar performance (≈ 22.2 – 22.3%), which is better than using no novel encoders at all (MoDAL-1: 22.4% in Table 1) but worse than the full three-encoder model (21.6%). This indicates that $BE^{(1)}$ and $BE^{(2)}$ each contribute complementary information that the other does not fully recover—consistent with their different input compositions (area 6v+44 spike power vs. area 44 only).

Replacing $BE^{(1,2)}$ with a second area 6v encoder $BE^{(0)'}$ (row 4) performs worst among the two-encoder configurations (22.5%), confirming that the benefit of additional encoders depends on access to area 44 signals, not merely on added model capacity. Additional component ablations (ResCNN, dropout, batch size, LLM choice, learning rate) are reported in Appendix C.

Table 4: Mean squared diagonal cross-correlation $\frac{1}{D} \sum_i (C_{ii}^{(m,n)})^2$ between modality pairs on the test set ($D=D_{\text{MoDAL}}=8192$, $B_{\text{test}}=880$). Lower is better.

Configuration \ Pair	(0, 1) ↓	(0, 2) ↓	(1, 2) ↓
1. No \mathcal{L}_{dec}	.085	.044	.197
2. Separate proj.	.081	.044	.213
3. MoDAL-Full	.003	.004	.015

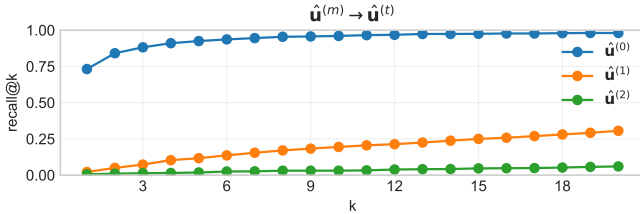


Figure 2: Neural-to-text retrieval recall@k in the MoDAL space for each modality on the test set ($n = 880$).

4.4 Analysis of Discovered Modalities

4.4.1 Decorrelation in the MoDAL Space. To verify that the decorrelation loss produces meaningfully different representations, we measure the mean squared diagonal cross-correlation $\frac{1}{D_{\text{MoDAL}}} \sum_i (C_{ii}^{(m,n)})^2$ between each modality pair in the full $D_{\text{MoDAL}} = 8192$ -dimensional MoDAL space on the test set. This is the quantity minimized by \mathcal{L}_{dec} ; lower values indicate greater decorrelation. We compare three configurations: (i) no decorrelation loss ($\lambda_{\text{dec}} = 0$), (ii) decorrelation through a separate projector (not shared with the contrastive loss), and (iii) MoDAL-Full with decorrelation in the shared projection space.

Table 4 reveals two findings. First, projecting into separate contrastive and decorrelation spaces (row 2) produces cross-correlations nearly identical to no decorrelation (row 1), confirming the trivial-collapse failure mode from Section 3.3.2: The projector satisfies \mathcal{L}_{dec} in its own space without propagating decorrelation pressure to the encoders. Second, the shared-space design (row 3) reduces cross-correlation by over an order of magnitude across all pairs, demonstrating that the contrastive loss prevents projector collapse and forces genuinely different encoder representations. The corresponding WER differences (Table 2) confirm that this decorrelation translates to improved downstream performance.

4.4.2 Contrastive Alignment Quality. We assess text–neural alignment quality in the MoDAL space using cosine-similarity retrieval and canonical correlation analysis (CCA).

Retrieval. For each modality m , we use the L2-normalized MoDAL projections $\hat{\mathbf{u}}_i^{(m)}$ as queries to retrieve the matched text projection $\hat{\mathbf{u}}_i^{(t)}$ from the full test set via cosine similarity, and report recall@k.

Figure 2 shows that $\text{BE}^{(0)}$ achieves strong sample-level alignment (recall@1 = 73%, recall@20 \approx 99%), expected given its rich temporal token sequence. $\text{BE}^{(1)}$ and $\text{BE}^{(2)}$ show substantially lower retrieval (recall@1 < 5%), but this is consistent with the MoDAL design: These encoders produce a single utterance-level vector and are explicitly

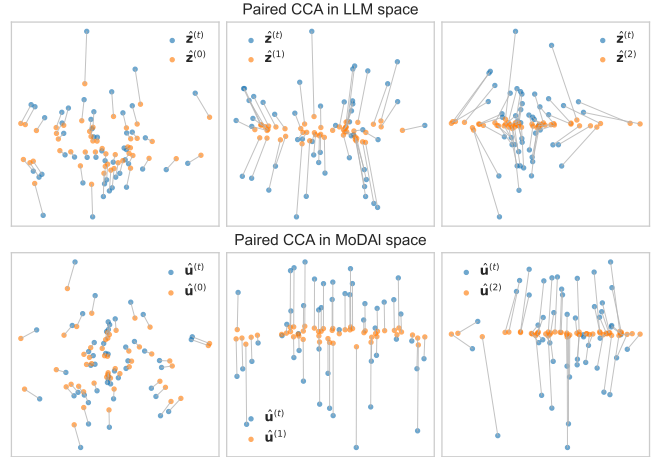


Figure 3: Paired CCA projections of neural and text representations. Top row: LLM embedding space ($\hat{\mathbf{z}}^{(m)}$ vs. $\hat{\mathbf{z}}^{(t)}$). Bottom row: MoDAL projection space ($\hat{\mathbf{u}}^{(m)}$ vs. $\hat{\mathbf{u}}^{(t)}$). Lines connect matched pairs ($n = 50$ subsampled for clarity).

trained via \mathcal{L}_{dec} to avoid encoding the same sample-discriminative information as $\text{BE}^{(0)}$. Their role is as *complementary conditioning signals* for the LLM—not standalone sample identifiers—confirmed by the WER improvement from MoDAL-1 to MoDAL-Full (Table 1) and the linguistic probe results below (Table 5).

Paired CCA. To visualize the geometric relationship between neural and text representations beyond cosine retrieval, we apply CCA [14] to each neural–text pair. Let $\hat{\mathbf{z}}_i^{(m)} = \bar{\mathbf{z}}_i^{(m)} / \|\bar{\mathbf{z}}_i^{(m)}\|$ denote the L2-normalized pooled representation in LLM space (before MoDAL projection). CCA finds linear projections of the neural and text matrices into a shared 2-D subspace that maximizes pairwise correlation. We apply it separately to the LLM-space pairs ($\hat{\mathbf{z}}^{(m)}$, $\hat{\mathbf{z}}^{(t)}$) and the MoDAL-space pairs ($\hat{\mathbf{u}}^{(m)}$, $\hat{\mathbf{u}}^{(t)}$). Lines connect matched neural–text samples; shorter lines indicate tighter alignment.

Figure 3 compares alignment before (top, LLM space) and after (bottom, MoDAL space) projection. In the LLM space, $\text{BE}^{(0)}$ shows moderate correspondence and the novel modalities show noisy alignment. After projection, the structure sharpens: $\text{BE}^{(0)}$ exhibits tight pairing (short lines), while $\text{BE}^{(1)}$ and $\text{BE}^{(2)}$ reveal organized geometric patterns with systematic neural–text correspondence that is not visible in the LLM space. This confirms that the MoDAL projection concentrates representational variance onto text-relevant directions, successfully extracting structure from the novel encoders that exists in the high-dimensional LLM embeddings but is not apparent without the learned projection.

4.4.3 Representational Diversity. To investigate whether the discovered modalities encode different linguistic information, we train linear probes [1] on the L2-normalized MoDAL projections $\hat{\mathbf{u}}_i^{(m)}$ for each brain encoder and the text projection $\hat{\mathbf{u}}_i^{(t)}$ as a reference. For each sentence in the test set ($n = 880$), we extract eight linguistic properties from the ground-truth transcription using a rule-based grammar detector. For classification targets (person, transitivity,

Table 5: Linear probe scores on linguistic properties. Bold: best neural modality per row. Italics: second best. The text column ($\hat{u}^{(t)}$) serves as a reference. Classification targets report accuracy; length reports R^2 .

Property	Metric \uparrow	$\hat{u}^{(0)}$	$\hat{u}^{(1)}$	$\hat{u}^{(2)}$	$\hat{u}^{(t)}$
Length	R^2	.67	.87	.75	.75
Voice	Acc	.90	.95	.95	.91
Wh-word	Acc	.85	.90	.90	.98
Determiner	Acc	.79	.83	.83	.85
Person	Acc	.74	.71	.59	.85
Aspect	Acc	.65	.68	.67	.69
Tense	Acc	.54	.49	.50	.73
Transitivity	Acc	.42	.40	.34	.48

tense, aspect, voice, determiner, wh-word) we fit a RidgeClassifier with stratified 5-fold cross-validation and report accuracy; for the regression target (sentence length) we fit Ridge regression ($\alpha=1.0$) and report R^2 . All results are significant at $p < 10^{-3}$ (one-sample t -test against chance). Full details including class labels and per-fold standard deviations are given in Table 8 (Appendix D).

Table 5 reveals clear linguistic specialization. The novel encoders BE⁽¹⁾ (area 6v+44 spike power) and BE⁽²⁾ (area 44) achieve the highest neural scores on structural and syntactic properties: sentence length ($R^2 = .87$ for BE⁽¹⁾, far exceeding even the text reference), grammatical voice (95% for both), wh-word presence (90%), and determiner type (83%). By contrast, BE⁽⁰⁾ (area 6v) excels at grammatical person (74% vs. 71% and 59%) and tense (54% vs. 49% and 50%); these are grammatical properties, but can be reliably inferred from articulatory patterns, since English pronouns (e.g., *I, you*) and tense morphology (e.g., *-d*) are distinguishable from their articulatory signatures alone.

This pattern aligns with the neurolinguistic understanding of these cortical regions: Area 6v encodes motor commands for speech production, while area 44 (Broca’s area) is associated with higher-level syntactic and structural processing. The MoDAL framework successfully recovers this functional distinction without any explicit supervision over which linguistic properties each encoder should capture. Notably, BE⁽¹⁾ achieves $R^2 = .87$ on sentence length—substantially higher than the text reference (.75)—suggesting that this encoder captures temporal extent information from the neural signal that is not linearly accessible from pooled text embeddings.

5 Conclusion

We presented MoDAL, a framework for self-supervised neural modality discovery that combines contrastive alignment and decorrelation in a shared projection space. The core insight is that these two objectives are in productive tension: Contrastive alignment anchors all brain encoders to text but transitively drives them to coalesce, while decorrelation counteracts this coalescence, forcing each encoder to specialize in different text-relevant information. We proved that this tension is inherent to the shared-space design (Propositions 3.1–3.2) and showed empirically that both

components—and their co-location in a single projection space—are necessary for the framework to discover useful modalities.

Applied to the Brain-to-Text Benchmark ’24, MoDAL achieved 21.6% WER, a 4.7 percentage point improvement over the previous best E2E method. The central finding is that area 44 (Broca’s area) signals—discarded as uninformative by all prior work on this dataset—carry complementary linguistic information that the MoDAL framework can discover and exploit. The contribution is both quantitative and qualitative: Beyond the WER reduction, linear probes reveal that the novel encoders surface syntactic and structural properties from area 44 that are complementary to the articulatory features captured by the primary encoder and not linearly accessible from text embeddings alone, consistent with the known neurolinguistic roles of these cortical regions.

Several directions remain open. The current system uses three parallel encoders; scaling to more could reveal additional modalities. The underlying mechanism—contrastive alignment with decorrelation for modality discovery—is domain-agnostic and could apply wherever intercorrelated signals must be decomposed into complementary representations, such as multi-sensor physiological monitoring or multi-region neural recordings for other cognitive tasks. Finally, complementary decoding strategies such as language model re-ranking could be applied on top of MoDAL to further close the gap with cascaded systems.

Safe and Responsible Innovation Statement

This work aims to restore communication for individuals with speech-impairing conditions such as ALS, directly supporting the inclusivity of multimodal interaction. The neural data used are from a publicly available, de-identified benchmark dataset collected with informed consent under institutional review [24]. Because neural signals may carry information beyond what participants intend to communicate, future deployments of speech BCIs must ensure that users retain control over when decoding is active and what is shared. The MoDAL framework’s ability to discover latent neural modalities underscores this concern: Decoded representations may reflect cognitive states beyond intended speech, and safeguards against unauthorized or covert decoding are essential. We encourage the community to develop consent frameworks and privacy protections that evolve alongside the increasing capability of neural decoding systems.

Acknowledgments

This research was funded by the Defense Advanced Research Projects Agency (DARPA), under contract W912CG23C0031.

References

- [1] Guillaume Alain and Yoshua Bengio. 2018. Understanding intermediate layers using linear classifier probes. doi:10.48550/arXiv.1610.01644 arXiv:1610.01644 [stat].
- [2] Jimmy Lei Ba, Jamie Ryan Kiros, and Geoffrey E. Hinton. 2016. Layer Normalization. doi:10.48550/arXiv.1607.06450 arXiv:1607.06450 [stat].
- [3] Alexei Baevski, Henry Zhou, Abdelrahman Mohamed, and Michael Auli. 2020. wav2vec 2.0: a framework for self-supervised learning of speech representations. In *Proceedings of the 34th International Conference on Neural Information Processing Systems (NIPS ’20)*. Curran Associates Inc., Red Hook, NY, USA, 12449–12460. <https://dl.acm.org/doi/10.5555/3495724.3496768>
- [4] Nicholas S. Card, Maitreyee Wairagkar, Carrina Jacobacci, Xianda Hou, Tyler Singer-Clark, Francis R. Willett, Erin M. Kunz, Chaofei Fan, Maryam Vahdati Nia, Darrel R. Deo, Aparna Srinivasan, Eun Young Choi, Matthew F. Glasser,

- Leigh R. Hochberg, Jaimie M. Henderson, Kiarash Shahlaie, Sergey D. Stavisky, and David M. Brandman. 2024. An Accurate and Rapidly Calibrating Speech Neuroprosthesis. *New England Journal of Medicine* 391, 7 (Aug. 2024), 609–618. doi:10.1056/NEJMoa2314132
- [5] Yunfei Chu, Jin Xu, Qian Yang, Haojie Wei, Xipin Wei, Zhifang Guo, Yichong Leng, Yuanjun Lv, Jinzheng He, Junyang Lin, Chang Zhou, and Jingren Zhou. 2024. Qwen2-Audio Technical Report. doi:10.48550/arXiv.2407.10759 arXiv:2407.10759 [eess].
- [6] Steven Kyle Crawford. 2023. grammar-detector: A grammatical feature detector for analyzing sentences, clauses, and phrases. <https://github.com/SKCrawford/grammar-detector>
- [7] Tim Dettmers, Artidoro Pagnoni, Ari Holtzman, and Luke Zettlemoyer. 2023. QLoRA: efficient finetuning of quantized LLMs. In *Proceedings of the 37th International Conference on Neural Information Processing Systems (NIPS '23)*. Curran Associates Inc., Red Hook, NY, USA, 10088–10115.
- [8] Sheng Feng, Heyang Liu, Yu Wang, and Yanfeng Wang. 2024. Towards an End-to-End Framework for Invasive Brain Signal Decoding with Large Language Models. In *Interspeech 2024*. International Speech Communication Association, Kos Island, Greece, 1495–1499. doi:10.21437/Interspeech.2024-382 arXiv:2406.11568 [cs].
- [9] Tobias Fiedler, Leon Hermann, Florian Müller, Sarel Cohen, Peter Chin, Tobias Friedrich, and Eilon Vaadia. 2025. Teaching Wav2Vec2 the Language of the Brain. doi:10.48550/arXiv.2501.09459 arXiv:2501.09459 [cs].
- [10] Adeen Flinker, Anna Korzeniewska, Avgusta Y. Shestyuk, Piotr J. Franaszczuk, Nina F. Dronkers, Robert T. Knight, and Nathan E. Crone. 2015. Redefining the role of Broca’s area in speech. *Proceedings of the National Academy of Sciences of the United States of America* 112, 9 (March 2015), 2871–2875. doi:10.1073/pnas.1414491112
- [11] Yariv Gal and Zoubin Ghahramani. 2016. Dropout as a Bayesian Approximation: Representing Model Uncertainty in Deep Learning. In *Proceedings of The 33rd International Conference on Machine Learning*. PMLR, 1050–1059. <https://proceedings.mlr.press/v48/gal16.html>
- [12] Rohit Girdhar, Alaeldin El-Nouby, Zhuang Liu, Mannat Singh, Kalyan Vasudev Alwala, Armand Joulin, and Ishan Misra. 2023. ImageBind: One embedding space to bind them all. In *CVPR*. doi:10.1109/CVPR52729.2023.01457
- [13] Alex Graves, Santiago Fernández, Faustino Gomez, and Jürgen Schmidhuber. 2006. Connectionist temporal classification: labelling unsegmented sequence data with recurrent neural networks. In *Proceedings of the 23rd international conference on Machine learning (ICML '06)*. Association for Computing Machinery, New York, NY, USA, 369–376. doi:10.1145/1143844.1143891
- [14] Harold Hotelling. 1936. Relations Between Two Sets of Variates. *Biometrika* 28, 3/4 (1936), 321–377. doi:10.2307/2333955
- [15] Edward J. Hu, Yelong Shen, Phillip Wallis, Zeyuan Allen-Zhu, Yuanzhi Li, Shean Wang, Lu Wang, and Weizhu Chen. 2021. LoRA: Low-Rank Adaptation of Large Language Models. doi:10.48550/arXiv.2106.09685 arXiv:2106.09685 [cs].
- [16] Bo Li, Chen Change Loy, Fanyi Pu, Jingkang Yang, Kaichen Zhang, Kairui Hu, Luu Minh Thang, Nguyen Quang Trung, Pham Ba Cong, Shuai Liu, Yezhen Wang, and Ziwei Liu. 2025. Aero-1-Audio. https://www.lmms-lab.com/posts/aero_audio/
- [17] Jingyuan Li, Trung Le, Chaofei Fan, Mingfei Chen, and Eli Shlizerman. 2025. Brain-to-text decoding with context-aware neural representations and large language models. *Journal of Neural Engineering* 22, 5 (Oct. 2025), 056026. doi:10.1088/1741-2552/adb1
- [18] Ilya Loshchilov and Frank Hutter. 2019. Decoupled Weight Decay Regularization. doi:10.48550/arXiv.1711.05101 arXiv:1711.05101 [cs].
- [19] Sean L. Metzger, Kaylo T. Littlejohn, Alexander B. Silva, David A. Moses, Margaret P. Seaton, Ran Wang, Maximilian E. Dougherty, Jessie R. Liu, Peter Wu, Michael A. Berger, Inga Zhuravleva, Adelyn Tu-Chan, Karunesh Ganguly, Gopala K. Anumanchipalli, and Edward F. Chang. 2023. A high-performance neuroprosthesis for speech decoding and avatar control. *Nature* 620, 7976 (Aug. 2023), 1037–1046. doi:10.1038/s41586-023-06443-4
- [20] Aaron van den Oord, Yazhe Li, and Oriol Vinyals. 2019. Representation Learning with Contrastive Predictive Coding. doi:10.48550/arXiv.1807.03748 arXiv:1807.03748 [cs].
- [21] Alec Radford, Jong Wook Kim, Chris Hallacy, Aditya Ramesh, Gabriel Goh, Sandhini Agarwal, Girish Sastry, Amanda Askell, Pamela Mishkin, Jack Clark, Gretchen Krueger, and Ilya Sutskever. 2021. Learning Transferable Visual Models From Natural Language Supervision. doi:10.48550/arXiv.2103.00020 arXiv:2103.00020 [cs].
- [22] Alexander B. Silva, Kaylo T. Littlejohn, Jessie R. Liu, David A. Moses, and Edward F. Chang. 2024. The speech neuroprosthesis. *Nature reviews. Neuroscience* 25, 7 (July 2024), 473–492. doi:10.1038/s41583-024-00819-9
- [23] Maxime Verwoert, Joaquín Amigó-Vega, Yingming Gao, Maarten C. Ottenhoff, Pieter L. Kubben, and Christian Herff. 2025. Whole-brain dynamics of articulatory, acoustic and semantic speech representations. *Communications Biology* 8, 1 (March 2025), 432. doi:10.1038/s42003-025-07862-x
- [24] Francis R. Willett, Erin M. Kunz, Chaofei Fan, Donald T. Avansino, Guy H. Wilson, Eun Young Choi, Foram Kamdar, Matthew F. Glasser, Leigh R. Hochberg,

Shaul Druckmann, Krishna V. Shenoy, and Jaimie M. Henderson. 2023. A high-performance speech neuroprosthesis. *Nature* 620, 7976 (Aug. 2023), 1031–1036. doi:10.1038/s41586-023-06377-x

- [25] Jure Zbontar, Li Jing, Ishan Misra, Yann LeCun, and Stéphane Deny. 2021. Barlow Twins: Self-Supervised Learning via Redundancy Reduction. doi:10.48550/arXiv.2103.03230 arXiv:2103.03230 [cs].
- [26] Yizi Zhang, Linyang He, Chaofei Fan, Tingkai Liu, Han Yu, Trung Le, Jingyuan Li, Scott Linderman, Lea Duncker, Francis R. Willett, Nima Mesgarani, and Liam Paninski. 2025. Decoding inner speech with an end-to-end brain-to-text neural interface. doi:10.48550/arXiv.2511.21740 arXiv:2511.21740 [cs].

A Proofs

PROOF OF PROPOSITION 3.1. Fix modality m . Rewrite the per-sample neural-to-text loss as

$$\ell_i^{(m \rightarrow t)} = \log \left(1 + \sum_{j \neq i} e^{(\hat{u}_i^{(m)} \cdot \hat{u}_j^{(t)} - \hat{u}_i^{(m)} \cdot \hat{u}_i^{(t)})/\tau} \right) \geq 0,$$

and likewise $\ell_i^{(t \rightarrow m)} \geq 0$ for the text-to-neural direction. Since $\mathcal{L}_{\text{con}}^{(m)}$ averages these non-negative terms, $\mathcal{L}_{\text{con}}^{(m)} \geq 0$.

Step 1: The configuration $\hat{u}_i^{(m)} = \hat{u}_i^{(t)}$ for all i drives $\mathcal{L}_{\text{con}}^{(m)}$ to zero. Under this assignment, the positive-pair similarity is $\hat{u}_i^{(t)} \cdot \hat{u}_i^{(t)} = 1$, and every negative-pair similarity satisfies $\hat{u}_i^{(t)} \cdot \hat{u}_j^{(t)} < 1$ by the distinctness assumption. Define $\delta^* = \min_i (1 - \max_{j \neq i} \hat{u}_i^{(t)} \cdot \hat{u}_j^{(t)}) > 0$. Each negative-pair exponent is at most $-\delta^*/\tau$, so using $\log(1 + x) \leq x$:

$$\ell_i^{(m \rightarrow t)} \Big|_{\hat{u}_i^{(m)} = \hat{u}_i^{(t)}} \leq (B - 1) e^{-\delta^*/\tau} \xrightarrow{\tau \rightarrow 0^+} 0.$$

The same bound holds for $\ell_i^{(t \rightarrow m)}$, so $\mathcal{L}_{\text{con}}^{(m)} = O(e^{-\delta^*/\tau}) \rightarrow 0$.

Step 2: Any configuration with $\hat{u}_k^{(m)} \neq \hat{u}_k^{(t)}$ for some k has strictly larger loss. The text-to-neural loss for sample i can be rewritten as

$$\ell_i^{(t \rightarrow m)} = \log(1 + C_i e^{-\hat{u}_i^{(t)} \cdot \hat{u}_i^{(m)}/\tau}), \quad \text{where } C_i = \sum_{j \neq i} e^{\hat{u}_i^{(t)} \cdot \hat{u}_j^{(m)}/\tau} > 0$$

is independent of $\hat{u}_i^{(m)}$. Since $a \mapsto \log(1 + C e^{-a})$ is strictly decreasing for $C > 0$, the loss $\ell_i^{(t \rightarrow m)}$ is strictly decreasing in $\hat{u}_i^{(t)} \cdot \hat{u}_i^{(m)}$. By Cauchy–Schwarz, $\hat{u}_i^{(t)} \cdot \hat{u}_i^{(m)} \leq 1$ with equality if and only if $\hat{u}_i^{(m)} = \hat{u}_i^{(t)}$. Therefore, for any fixed $\{\hat{u}_j^{(m)}\}_{j \neq i}$:

$$\ell_i^{(t \rightarrow m)} \Big|_{\hat{u}_i^{(m)} \neq \hat{u}_i^{(t)}} > \ell_i^{(t \rightarrow m)} \Big|_{\hat{u}_i^{(m)} = \hat{u}_i^{(t)}}. \quad (1)$$

Now suppose $\hat{u}_k^{(m)} \neq \hat{u}_k^{(t)}$ for some index k , and let $\epsilon = 1 - \hat{u}_k^{(t)} \cdot \hat{u}_k^{(m)} > 0$. We quantify how much worse the loss is. At the optimum ($\hat{u}_k^{(m)} = \hat{u}_k^{(t)}$), the k -th text-to-neural term is

$$\ell_k^{(t \rightarrow m)} \Big|_{\text{opt}} = \log(1 + C_k^* e^{-1/\tau}),$$

where $C_k^* = \sum_{j \neq k} e^{\hat{u}_k^{(t)} \cdot \hat{u}_j^{(t)}/\tau}$. At the suboptimal point, the same term is

$$\ell_k^{(t \rightarrow m)} = \log(1 + C_k e^{-(1-\epsilon)/\tau}).$$

The ratio of the arguments inside $\log(1 + \cdot)$ satisfies

$$\frac{C_k e^{-(1-\epsilon)/\tau}}{C_k^* e^{-1/\tau}} = \frac{C_k}{C_k^*} e^{\epsilon/\tau} \xrightarrow{\tau \rightarrow 0^+} \infty,$$

since C_k/C_k^* is bounded away from zero (both are positive sums of the same number of terms with bounded exponents). Therefore $\ell_k^{(t \rightarrow m)}$ is exponentially larger than $\ell_k^{(t \rightarrow m)}|_{\text{opt}}$ as $\tau \rightarrow 0$.

Since all $2B$ per-sample terms $(\ell_i^{(m \rightarrow t)})$ and $\ell_i^{(t \rightarrow m)}$ for each i are non-negative, no improvement in the remaining terms can compensate for the exponential excess in $\ell_k^{(t \rightarrow m)}$. The total loss $\mathcal{L}_{\text{con}}^{(m)}$ at the suboptimal configuration thus strictly exceeds the optimum for all sufficiently small τ .

Conclusion. Since this holds for each modality m independently and \mathcal{L}_{con} averages over modalities, the unique minimizer is $\hat{\mathbf{u}}_i^{(m)} = \hat{\mathbf{u}}_i^{(t)}$ for all $m \in [M]$ and $i \in [B]$. The transitivity conclusion $\hat{\mathbf{u}}_i^{(m)} = \hat{\mathbf{u}}_i^{(n)}$ follows immediately. \square

PROOF OF PROPOSITION 3.2. If $\hat{\mathbf{u}}_i^{(m)} = \hat{\mathbf{u}}_i^{(n)}$ for all i , then the columns $[\hat{\mathbf{u}}_1^{(m)}, \dots, \hat{\mathbf{u}}_B^{(m)}]^\top$ and $[\hat{\mathbf{u}}_1^{(n)}, \dots, \hat{\mathbf{u}}_B^{(n)}]^\top$ are identical matrices. Since batch standardization is a deterministic column-wise affine transformation, $\check{\mathbf{U}}^{(m)} = \check{\mathbf{U}}^{(n)}$. Therefore, for each feature i ,

$$C_{ii}^{(m,n)} = \frac{1}{B} \sum_{k=1}^B \check{U}_{ki}^{(m)} \check{U}_{ki}^{(n)} = \frac{1}{B} \sum_{k=1}^B (\check{U}_{ki}^{(m)})^2 = 1,$$

where the last equality follows from the unit-variance property of batch standardization. \square

B Hyperparameters

Table 6 lists all hyperparameters used in the final model. Stage 1 and Stage 2 share the same brain encoder architecture; differences are noted where applicable.

C Additional Component Ablations

Table 7 reports ablations of engineering components not directly related to the modality discovery mechanism.

The ResCNN on $\text{BE}^{(0)}$ contributes substantially (25.0% without vs. 21.6% with), confirming that the temporal refinement of articulatory features is important for the LLM decoder. Channel-wise locked dropout is critical (26.4% without), consistent with its role in preventing electrode overfitting across recording sessions. LayerNorm on the GRU output has a modest effect (22.1% vs. 21.6%).

Using Qwen2-Audio-7B-Instruct [5] as the LLM decoder degrades performance to 27.6%. The larger model requires substantially more GPU memory, preventing us from increasing the LoRA rank beyond $r=16$ or the batch size beyond $B=128$ under our hardware constraints. A higher-capacity adapter and larger batches may be necessary to effectively adapt a 7B model with QLoRA on this dataset; we leave this exploration to future work.

Halving the batch size from 128 to 64 degrades WER to 23.9%. Both the contrastive and decorrelation losses benefit from larger batches: The InfoNCE objective requires sufficient in-batch negatives for effective sample discrimination, and the cross-correlation matrix in \mathcal{L}_{dec} provides more stable estimates of inter-modality feature correlation with more samples.

Using a single learning rate for all Stage 2 modules (1.5×10^{-4} or 2×10^{-4}) slightly degrades performance to 22.2% in both cases,

Table 6: Hyperparameters for the final MoDAL model.

Hyperparameter	Value
<i>Brain encoder (all stages)</i>	
Input kernel size k / stride s	14 / 4
Channel-wise locked dropout	0.75
BiGRU layers	5
GRU hidden dim (per direction)	512
GRU dropout	0.75
<i>ResCNN (Stage 2, $\text{BE}^{(0)}$ only)</i>	
Conv kernel size / dilation	5 / 2
<i>LLM decoder (Stage 2)</i>	
LLM embedding dim D_{LLM}	1536
QLoRA quantization	NF4, double quant
LoRA rank r / scaling α	16 / 32
LoRA dropout	0.15
LoRA target modules	all *_proj layers
<i>MoDAL projection (Stage 2)</i>	
MoDAL projection dim D_{MoDAL}	8192
Projector type	Affine
Temperature τ (initial)	0.1
λ_{con} (final)	1.0
λ_{dec} (final)	2.0
<i>Optimization</i>	
Optimizer	AdamW
(β_1, β_2)	(0.9, 0.999)
Weight decay	10^{-2}
LR schedule	Cosine annealing
Peak LR (Stage 1)	1×10^{-4}
Peak LR (Stage 2, $\text{BE}^{(0)}$ only)	1.5×10^{-4}
Peak LR (Stage 2, others)	2.0×10^{-4}
Batch size	128
Stage 1 epochs	300
Stage 2 epochs	150
Gradient clipping	10.0

Table 7: Additional component ablations on the test set. WER (%) is mean \pm 95% CI over 5 seeds. MoDAL-Full (21.6 \pm 0.1) is the reference.

Configuration	Test WER \downarrow
w/o ResCNN	25.0 \pm 0.2
w/o LayerNorm on GRU	22.1 \pm 0.2
w/o Drop _{chan}	26.4 \pm 0.3
LLM=Qwen2-Audio-7B-Instruct	27.6 \pm 0.4
Batch size $B=64$	23.9 \pm 0.3
Single LR (1.5×10^{-4})	22.2 \pm 0.2
Single LR (2×10^{-4})	22.2 \pm 0.2

confirming that the decoupled schedule—slower for pretrained components, faster for randomly initialized ones—provides a modest but consistent benefit.

D Linear Probe Details

Table 8 reports the full linear probe results. All probes operate on the L2-normalized MoDAI projections ($\hat{\mathbf{u}}^{(m)}$ for neural, $\hat{\mathbf{u}}^{(t)}$ for text) from the test set (880 sentences). Linguistic properties are extracted from ground-truth transcriptions using the grammar-detector Python library [6]. Sentences for which parsing fails (19 out of 880) receive default none labels (e.g., a short utterance like ‘summary points’ does not have tense). For classification, we use `RidgeClassifier` with `StandardScaler` and stratified 5-fold cross-validation, reporting accuracy. For regression (sentence length), we use `Ridge` ($\alpha = 1.0$) with `StandardScaler` and 5-fold cross-validation, reporting R^2 . p -values are computed via one-sample t -test of the 5 fold scores against the chance baseline (uniform accuracy $1/|\text{classes}|$ for classification, $R^2 = 0$ for regression).

Table 8: Full linear probe results. Score is mean \pm std over 5 folds. All $p < 10^{-3}$.

Property	Task	Classes / Range	$\hat{u}^{(0)}$	$\hat{u}^{(1)}$	$\hat{u}^{(2)}$
Length	Regression	2–17 words	.67 \pm .03	.87 \pm .02	.75 \pm .03
Voice	Classification	active, passive, none	.90 \pm .01	.95 \pm .00	.95 \pm .00
Wh-word	Classification	true, false	.85 \pm .04	.90 \pm .01	.90 \pm .01
Determiner	Classification	definite, indefinite, other, none	.79 \pm .02	.83 \pm .01	.83 \pm .01
Person	Classification	1st, 2nd, 3rd, none	.74 \pm .03	.71 \pm .02	.59 \pm .02
Aspect	Classification	simple, continuous, perfect, none	.65 \pm .03	.68 \pm .02	.67 \pm .02
Tense	Classification	past, present, future, none	.54 \pm .02	.49 \pm .04	.50 \pm .03
Transitivity	Classification	intransitive, transitive, ditransitive, impersonal, none	.42 \pm .01	.40 \pm .03	.34 \pm .03